The Neuroradiology Journal 27: 616-626, 2014 - doi: 10.15274/NRJ-2014-10055 www.centauro.it

Diffusion Tensor Imaging of Neurofibromatosis Bright Objects in Children with Neurofibromatosis Type 1

GULHAN ERTAN[1], ELCIN ZAN[2], DAVID M. YOUSEM[2], CAN CERITOGLU[3], AYLIN TEKES[1], ANDREA PORETTI[1], THIERRY A.G.M HUISMAN[1]

[1] Division of Pediatric Radiology, [2] Division of Neuroradiology, Russell H. Morgan Department of Radiology and Radiological Science, The Johns Hopkins University School of Medicine; Baltimore, MD, USA
[3] The Center for Imaging Science, The Johns Hopkins University; Baltimore, MD, USA

Key words: diffusion tensor imaging, neurofibromatosis type 1, neurofibromatosis bright objects, fiber tractography, children

SUMMARY – *Neurofibromatosis bright objects (NBOs) are poorly understood. This article aimed to investigate: 1) differences in fractional anisotropy (FA) between NBOs based in gray matter (GM) and white matter (WM), and 2) the relationship between NBOs and the affected white matter tracts. Fourteen NF1 patients were included in this study. Apparent diffusion coefficient (ADC), FA, radial diffusivity (RD) and eigenvalues were used to compare NBOs and matching contralateral normal-appearing sites (NAS). Diffusion tensor imaging scalars were also compared with age-matched healthy controls. Fiber tractography was performed to assess NBO-induced changes in WM trajectories. ADC values were higher for GM and WM NBOs than for NAS and controls. FA values were lower in GM and WM NBOs compared with controls. In all regions, eigenvalues were higher in NBOs than in NAS and controls. Only three out of 18 NOBs appeared to disrupt WM tracts. ADC, λ_2 and RD values of WM NBOs were higher in symptomatic compared to asymptomatic patients. Increased ADC, RD and eigenvalues and decreased FA values in NBOs can be explained by myelin and axonal damage. Increased ADC values and RD in WM NBOs correlated with the presence of symptoms. Tract integrity predominated in our study.*

Introduction

Neurofibromatosis type 1 (NF1) is one of the most common genetic disorders with manifold manifestations affecting the central nervous system (CNS) [1]. Clinical findings vary significantly and range from focal neurological deficits like vision impairment, to more diffuse symptoms including intellectual disability with abnormal executive function, impaired attention and language deficits [2]. Neuroimaging may reveal low-grade gliomas mainly of the optic pathway, as well as within the brain stem and cerebellum [3]. In addition, cerebro-vasculopathies such as moyamoya syndrome may be observed [4].

One of the most intriguing NF1 lesions is the so-called "unidentified bright objects (UBOs) or neurofibromatosis bright objects (NBOs)" [5,6]. They are observed as ill-defined focal hyperintense lesions on T2-weighted and fluid attenuation inversion recovery (FLAIR) sequences within the deep gray matter, brain stem, and cerebellum, or along white matter (WM) tracts. They are reported in 43-93% of patients with NF1 [7,8]. These lesions have been variably classified as hamartomas, heterotopias, dysplastic areas, regions of de-/dysmyelination or glial nodules [9]. They are poorly understood, thought to be benign in scope and may regress over time or recur with advancing age [7,10].

NBOs most frequently reside in the striatocapsular region and along the course of major WM tracts [5,7,8,10]. Hence, they are ideally suited to be evaluated by diffusion tensor imaging (DTI). The small number of scientific papers evaluating NBOs by diffusion-weighted imaging have mostly focused on studying the appar-

ent diffusion coefficient (ADC) values of NBOs [11-14]. Few studies have evaluated the fractional anisotropy (FA) values and the corresponding eigenvalues of these lesions [15-19]. In addition, no study is available that systematically applied fiber tractography (FT) to the evaluation of NBOs and their relation to WM tracts within the brain.

The goal of our study is to corroborate the published DTI data on NBOs and to further clarify their significance. Particularly, we aim to investigate 1) differences in FA between NBOs in gray matter (GM) and WM, and 2) the relationship between NBOs and the affected WM tracts.

Material and Methods

Institutional review board approval was obtained for this retrospective Health Insurance Portability and Accountability Act compliant study, and a waiver of informed consent was granted.

Subjects

The inclusion criteria for this retrospective study were: 1) confirmed diagnosis of NF1, 2) availability of DTI data without artifacts enabling high quality DTI post-processing, and 3) availability of clinical records. Eligible patients were collected through an electronic search of our pediatric neuroradiology database covering a time period of 12 months. The following key words were used: neurofibromatosis 1, NF1, NBO or UBO. Demographic data and detailed information on the neurological features related to NF1 were collected from the electronic medical record.

Age- and gender-matched controls were selected from our pediatric MR database using the following criteria: (1) normal brain anatomy, (2) absence of neurological disorders, and (3) availability of DTI raw data.

Diffusion Tensor Imaging

All MRI studies were performed on a 1.5 T scanner (Siemens Avanto, Erlangen, Germany) using our standard departmental protocol including pre- and postcontrast 3D-T1-weighted and axial T2-weighted/FLAIR sequences, as well as a single-shot fast spin-echo, echo-planar axial DTI sequence with diffusion gradients along 20 independent non-collinear directions. An effective high b-value of 1000 s/mm^2 was used for each of the 20 diffusion-encoding directions. We performed an additional measurement without diffusion weighting (b=0 s/mm^2). For acquisition of the DTI data the following parameters were used: TR = 5500 ms, TE = 88 ms, slice thickness = 2.5 mm, FOV = 240×240 mm and matrix size = 96×96.

Qualitative Image Analysis

All patients were systematically evaluated for the presence, number, and location of NBOs by two experienced pediatric neuroradiologists in consensus (AT and TAGMH), blinded to the patients' symptoms. Focal lesions that appeared T2/FLAIR hyperintense and T1-isointense without focal contrast enhancement were classified as NBOs. When no focal T2/FLAIR hyperintense signal alteration was present and no contrast enhancement was noted, the area was scored as a normal-appearing site (NAS). The numbers of NBOs evaluated were limited to five per patient for the Purpose of the study. When patients had more than five NBOs, the largest five NBÒs were selected for data analysis.

Quantitative DTI Analysis

DTI data of the patients were transferred to an off-line workstation for further post-processing. DtiStudio, DiffeoMap and RoiEditor software (available at www.MriStudio.org) were used. Raw DTI images were first realigned to the B0 images for co-registration and eddy current distortion correction using the affine transformation of Automated Image Registration (AIR) package 20. The six independent elements of the diffusion tensor were calculated using multivariate linear fitting algorithm. The tensor was diagonalized to obtain three eigenvalues (λ_1, λ_2, λ_3) and corresponding eigenvectors (v_1, v_2, v_3). The eigenvector associated with the largest eigenvalue (v_1) was used as an indicator of fiber orientation. In addition, FA, ADC and radial diffusivity (RD) maps were computed.

The large deformation diffeomorphic metric mapping (LDDMM) algorithm was used to compute a nonlinear transformation between B_0 image representing the DTI data and the matching T2 image of each subject to correct for the geometric distortion caused by B_0 inhomogeneity during DTI data acquisition [21,22]. The transformation matrix obtained from LDDMM

mapping was applied to the DTI images to co-register DTI data and the T2-weighted images.

ADC, FA and eigenvalue (λ_1, λ_2, λ_3) measurements in NBOs and NAS were used for quantitative data analysis using the region-of-interest (ROI) approach. Care was taken that all measurements were performed within the NBOs and the exactly matching normal-appearing contralateral anatomical site. In controls, the ROIs were placed in the matching GM and WM regions compared to the age-matched patients.

Fiber Tractography

FT was performed using DtiStudio software to assess NBÒs-induced changes in WM integrity and trajectories. For the 3D tract reconstruction, the Fiber Assignment by Continuous Tractography (FACT) algorithm with the "brute-force" method was used [23-25]. A FA value of 0.2 and a principal eigenvector turning angle of 40° between two connected pixels were used as thresholds to terminate fiber tracking.

A multi-ROI approach was used to reconstruct tracts of interest depending on the location of NBÒs. For each tract, ROIs were manually defined according to well-established reproducible FT protocols [26]. When multiple ROIs were used for a tract of interest, three types of operations ("AND", "CUT" and "NOT") were employed [26].

Statistical Analysis

NBOs were examined and categorized as GM or WM NBOs. The average ADC, FA and eigenvalues (λ_1, λ_2, λ_3) for NBOs, NAS and controls were tested with the Kruskal-Wallis test (non-parametric one-way analysis of variance test) to compare the mean ROI values. A $p \leq 0.05$ was considered statistically significant. Subsequently, multiple comparisons using Bonferroni correction were made between GM and WM NBOs, NAS and controls. Data of subjects with and without neurological symptoms were analyzed for significant association between ADC, FA, RD and eigenvalues with the Wilcoxon rank-sum test.

Results

Patients

Within the 12 months survey period 263 children with a confirmed or suspected diagnosis of NF1 were treated in our tertiary pediatric hospital, 14/263 (5.3%, seven females) fulfilled the inclusion criteria. The mean age at MRI of the 14 patients was 7.2 ± 3.4 years.

Six out of 14 patients (43%) had one or more neurological symptoms including: gait disturbance (n=3), blurred vision without optic nerve pathology (n=2), epileptic seizures (n=2), swallowing difficulty (n=2), attention deficit hyperactivity disorder (n=1), autism (n=1), headaches (n=1), intellectual disability (n=1) and speech impairment (n=1). Eight out of 14 patients did not have any neurological symptoms but were imaged for screening Purposes.

Qualitative Image Analysis

In the 14 pediatric NF1 patients, qualitative MRI analysis detected 57 NBÒs in various locations. Thirty-one NBOs (54%) were located in the GM, 26 (46%) were in the WM. The distribution of the NBOs in the GM and MW, respec-

Table 1 The location and number of neurofibromatosis bright objects (NBOs) in gray matter.

Gray matter regions	*Number of NBOs*
Globi pallidi	12
Dentate nuclei	11
Subthalamic nuclei	3
Caudate nuclei	2
Cerebellar foliae	1
Putamina	1
Thalami	1
Total	31

Table 2 The location and number of neurofibromatosis bright objects (NBOs) in white matter.

White matter regions	*Number of NBOs*
Cerebellar peduncles	7
Pons	6
Corpus callosum	5
Internal capsules	3
Midbrain	2
Cerebellar white matter	1
Frontal white matter	1
Lower brain stem	1
Total	26

tively, are shown in Tables 1 and 2. The most common GM and WM locations for NBOs were: globi pallidi (n=12), dentate nuclei (n=11), cerebellar peduncles (n=7) and pontine white matter tracts (n=6).

Quantitative DTI Analysis

FA, ADC and RD values as well as eigenvalues (mean and standard deviation) of the GM and WM NBOs and NAS are listed in Tables 3 and 4. The measured values of the control DTI scalars in the matching GM and WM regions in the control subjects are also included. Kruskal-Wallis test showed at least one group mean rank significantly different from the others except for λ_1 in the WM. Results of multiple comparisons with Bonferroni correction between GM and WM NBOs, NAS and controls are shown in Figures 1 and 2.

For GM ROIs, multiple comparisons with Bonferroni correction showed that ADC, λ_1, λ_2, λ_3 and RD values were significantly higher in GM NBOs compared to NAS ($p<0.001$, <0.02,

Table 3 DTI scalars of different GM ROIs for NBOs, NASs and controls (mean value ± SD).

ROI	*n*	*Group*	*FA*	*ADC* ($\times10^{-3}mm^2/s$)	λ_1 ($\times10^{-3}mm^2/s$)	λ_2 ($\times10^{-3}mm^2/s$)	λ_3 ($\times10^{-3}mm^2/s$)	*RD* ($\times10^{-3}mm^2/s$)
GP	12	NBO	0.18±0.06	1.09±0.15	1.28±0.16	1.08±0.16	0.92±0.15	1.00±0.15
		NAS	0.23±0.09	0.91±0.10	1.08±0.11	0.92±0.12	0.75±0.12	0.83±0.11
		Control	0.25±0.07	0.89±0.08	1.10±0.10	0.89±0.10	0.67±0.09	0.78±0.09
DN	11	NBO	0.20±0.07	0.97±0.13	1.16±0.18	0.95±0.12	0.80±0.15	0.87±0.13
		NAS	0.24±0.13	0.84±0.09	1.12±0.18	0.80±0.11	0.61±0.11	0.70±0.10
		Control	0.38±0.16	0.78±0.09	1.12±0.21	0.70±0.13	0.52±0.16	0.61±0.13
SN	3	NBO	0.15±0.03	1.00±0.06	1.20±0.10	0.97±0.06	0.83±0.06	0.90±0.05
		NAS	0.28±0.21	0.99±0.04	1.27±0.06	0.93±0.06	0.77±0.06	0.85±0.05
		Control	0.24±0.11	0.92±0.12	1.18±0.28	0.84±0.07	0.74±0.03	0.79±0.05
CN	2	NBO	0.18±0.02	0.98±0.02	1.10±0.00	1.00±0.00	0.85±0.07	0.93±0.04
		NAS	0.24±0.06	0.87±0.05	1.00±0.00	0.85±0.07	0.75±0.07	0.80±0.07
		Control	0.14±0.02	0.78±0.00	0.89±0.01	0.78±0.01	0.67±0.01	0.72±0.00
C	1	NBO	0.14	0.90	1.20	0.80	0.70	0.75
		NAS	0.14	0.83	1.10	0.70	0.70	0.70
		Control	0.51	0.67	1.00	0.76	0.26	0.51
P	1	NBO	0.12	1.02	1.10	1.00	0.90	0.95
		NAS	0.13	0.89	0.90	0.80	0.70	0.75
		Control	0.17	0.84	0.99	0.83	0.71	0.77
T	1	NBO	0.26	1.00	1.20	0.90	0.70	0.80
		NAS	0.27	0.80	1.40	0.70	0.60	0.65
		Control	0.49	0.84	1.37	0.66	0.54	0.60
Total	31	NBO	0.18±0.06	1.02±0.14	1.21±0.16	1.00±0.14	0.85±0.14	0.92±0.14
		NAS	0.23±0.11	0.89±0.10	1.11±0.16	0.85±0.12	0.69±0.12	0.77±0.11
		Control	0.30±0.14	0.84±0.10	1.11±0.17	0.80±0.13	0.61±0.15	0.70±0.13

ADC, apparent diffusion coefficient; *C*, cerebellar foliae; *CN*, caudate nuclei; *DN*, dentate nuclei; *FA*, fractional anisotropy; *GM*, gray matter; *GP*, globi pallidi; *NAS*: normal-appearing site (contralateral to NBO); *NBO*, neurofibromatosis bright object; *P*, putamina; *RD*, radial diffusivity; *ROI*, region of interest; *SD*, standard deviation; *SN*, subthalamic nuclei; *T*, thalami.

<0.001, <0.001 and <0.001, respectively) and controls (p<0.001, 0.007, <0.001, <0.001 and <0.001, respectively). The trend for FA being lower was significant in GM NBOs when compared to controls (p<0.001), but the decrease was not significant when compared to NAS (p=0.184). ADC, λ_2, λ_3 and RD values were higher and FA values were lower in GM NAS compared to controls, but the differences were not statistically significant.

For WM ROIs, multiple comparisons with Bonferroni correction showed that ADC, λ_2, λ_3 and RD values were significantly higher in WM NBOs compared to NAS (p<0.001, <0.001, <0.001 and <0.001, respectively) and controls (p=0.022, <0.001, =0.002 and <0.001, respectively). The trend for FA being lower was significant in WM NBOs when compared to controls (p=0.002), but the decrease was not significant when compared to NAS (p=0.085). The values of λ_1 were higher in WM NBOs compared to NAS without statistical significance (p>0.005). Interestingly WM NBOs showed lower λ_1 values compared to controls (p>0.005). ADC, FA

Table 4 DTI scalars of different WM ROIs for NBOs, NASs and controls (mean value ± SD).

ROI	*n*	*Group*	*FA*	*ADC* ($\times 10^{-3} mm^2/s$)	λ_1 ($\times 10^{-3} mm^2/s$)	λ_2 ($\times 10^{-3} mm^2/s$)	λ_3 ($\times 10^{-3} mm^2/s$)	*RD* ($\times 10^{-3} mm^2/s$)
CP	7	NBO	0.31±0.11	1.00±0.10	1.27±0.15	0.94±0.08	0.79±0.11	0.86±0.09
		NAS	0.40±0.11	0.88±0.09	1.21±0.15	0.79±0.07	0.63±0.11	0.71±0.08
		Control	0.33±0.08	1.13±0.40	1.50±0.44	1.05±0.40	0.83±0.37	0.94±0.38
Pons	6	NBO	0.31±0.09	0.98±0.08	1.25±0.16	0.95±0.05	0.75±0.08	0.85±0.05
		NAS	0.34±0.12	0.86±0.03	1.13±0.05	0.83±0.05	0.62±0.08	0.73±0.03
		Control	0.32±0.06	0.98±0.20	1.31±0.26	0.91±0.17	0.70±0.19	0.81±0.18
CC	5	NBO	0.21±0.09	1.16±0.11	1.66±0.18	1.00±0.07	0.82±0.11	0.91±0.09
		NAS	0.31±0.09	0.92±0.05	1.58±0.13	0.68±0.08	0.50±0.10	0.59±0.09
		Control	0.63±0.06	0.92±0.12	1.68±0.15	0.62±0.13	0.46±0.11	0.54±0.12
PLIC	3	NBO	0.33±0.08	0.91±0.10	1.37±0.21	0.80±0.10	0.57±0.15	0.68±0.13
		NAS	0.40±0.11	0.90±0.10	1.30±0.10	0.83±0.06	0.57±0.15	0.70±0.10
		Control	0.46±0.11	0.81±0.06	1.26±0.09	0.67±0.10	0.49±0.11	0.58±0.10
MI	2	NBO	0.29±0.10	1.03±0.05	1.30±0.14	1.00±0.00	0.80±0.00	0.90±0.00
		NAS	0.50±0.21	0.95±0.07	1.25±0.21	0.90±0.00	0.70±0.00	0.80±0.00
		Control	0.40±0.09	0.90±0.00	1.34±0.12	0.76±0.09	0.61±0.04	0.68±0.06
CWM	1	NBO	0.12	1.07	1.50	0.90	0.80	0.85
		NAS	0.09	0.83	1.20	0.70	0.60	0.65
		Control	0.52	0.72	1.19	0.54	0.42	0.48
FWM	1	NBO	0.36	1.27	1.50	1.20	1.10	1.15
		NAS	0.45	1.10	1.40	1.10	0.80	0.95
		Control	0.45	0.87	1.34	0.74	0.54	0.64
LB	1	NBO	0.28	1.03	1.20	1.00	0.90	0.95
		NAS	0.26	0.93	1.00	0.90	0.90	0.90
		Control	0.16	2.28	2.66	2.15	2.03	2.09
Total	26	NBO	0.29±0.10	1.03±0.12	1.37±0.22	0.95±0.10	0.78±0.14	0.87±0.12
		NAS	0.36±0.13	0.90±0.08	1.28±0.20	0.80±0.11	0.62±0.13	0.71±0.11
		Control	0.41±0.14	1.02±0.36	1.48±0.38	0.88±0.38	0.69±0.37	0.79±0.38

ADC, apparent diffusion coefficient; *CC*, corpus callosum; *CP*, cerebellar peduncles; *CWM*, cerebellar white matter; *FA*, fractional anisotropy; *DWM*, frontal white matter; *LB*, lower brain stem; *MI*, midbrain; *NAS*: normal-appearing site (contralateral to NBO); *NBO*, neurofibromatosis bright object; *PLIC*, posterior limb of the internal capsule; *RD*, radial diffusivity; *ROI*, region of interest; *SD*, standard deviation; *WM*, white matter.

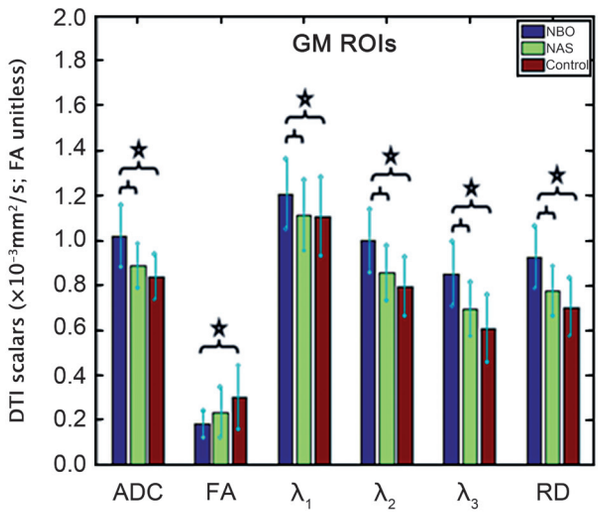

Figure 1 Box plot shows the differences in ADC, FA, eigenvalues and RD for GM ROIs of NBOs, NSAs and controls after Bonferroni correction. Statistically significant differences between groups are indicated with a star.

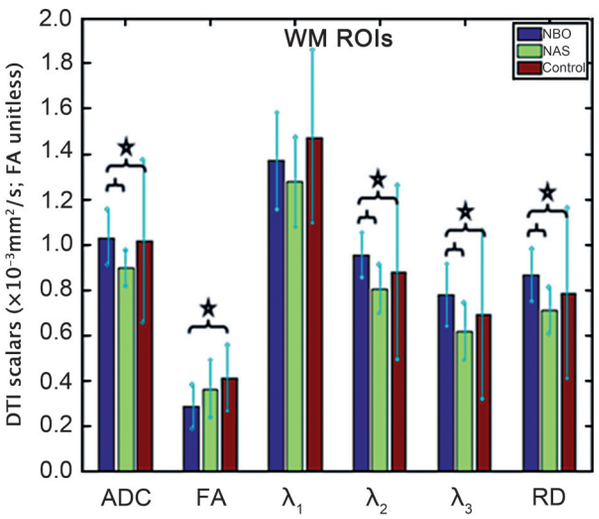

Figure 2 Box plot shows the differences in ADC, FA, eigenvalues and RD for WM ROIs of NBOs, NSAs and controls after Bonferroni correction. Statistically significant differences between groups are indicated with a star.

Table 5 Relationship between neurofibromatosis bright objects and adjacent white matter tracts.

Location of the NBO	*Adjacent WM tract*	*Location of the NBO compared to the WM tract*			*Impact on the WM tract*		
		Within	*Adjacent*	*Not related*	*No effect*	*Disruption*	*Displacement*
CN	ATR	+	–	–	+	–	–
MCP	MCP	+	–	–	+	–	–
ICP	ICP	+	–	–	+	–	–
SCP	SCP	+	–	–	+	–	–
PLIC	CBT	+	–	–	+	–	–
PLIC	CBT	+	–	–	+	–	–
PLIC	CBT	+	–	–	+	–	–
Pons	CST/CBT	+	–	–	–	+	–
Pons	CST/CBT	–	–	+	+	–	–
Pons	CST/CBT	+	–	–	+	–	–
Pons	CST/CBT	+	–	–	+	–	–
MI	CBT	+	–	–	+	–	–
GP	ATR	–	+	–	+	–	–
GP	ATR	+	–	–	+	–	–
DN	SCP	+	–	–	–	+	–
CC	Splenium	+	–	–	–	+	–
CC	Cingulum	+	–	–	+	–	–
FWM	ACR	+	–	–	+	–	–

ACR, anterior region of corona radiata; *ATR*, anterior thalamic radiation; *CBT*, corticobulbar tract; *CC*, corpus callosum; *CN*, caudate nucleus; *CST*, corticospinal tract; *DN*, dentate nucleus; *FWM*, frontal white matter; *GP*, globus pallidus; *ICP*, inferior cerebellar peduncle; *MCP*, middle cerebellar peduncle; *MI*, midbrain; *NBO*, neurofibromatosis bright object; *PLIC*, posterior limb of the internal capsule; *SCP*, superior cerebellar peduncle; *WM*, white matter.

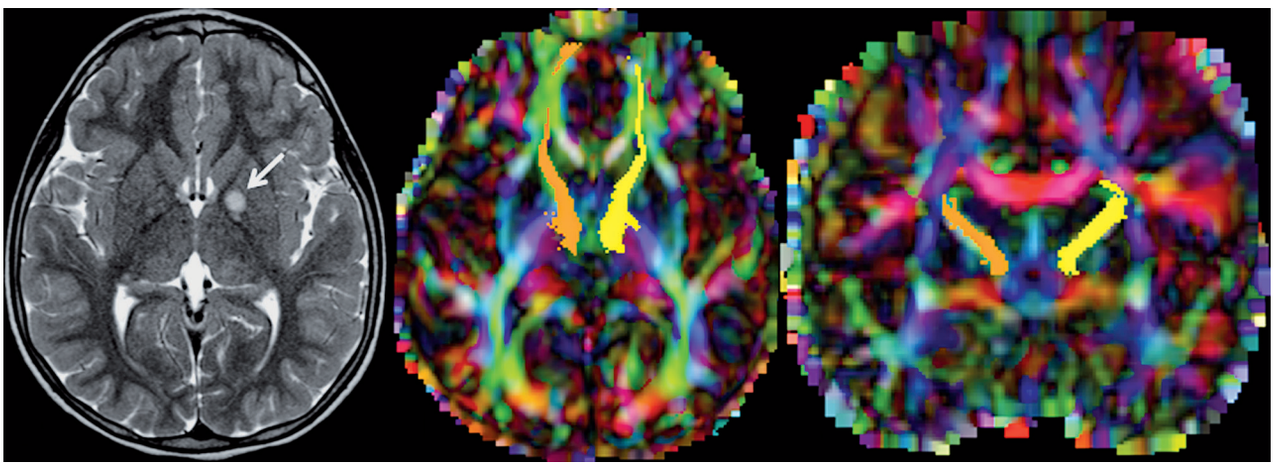

A B C

Figure 3 A) Axial T2-weighted image of patient 3 shows a NBO in the left globus pallidus (arrow). Axial (B) and coronal (C) color-coded FA maps with superimposed FT of the left (yellow) and right (orange) anterior thalamic radiations. The NBO in the left globus pallidus does not have any effect on the adjacent anterior thalamic radiation.

and eigenvalues (λ_1, λ_2, λ_3) were lower in WM NAS compared to controls, but the differences were not statistically significant.

No association was found between the neurological symptoms and ADC, FA and eigenvalues measurements of the GM NBOs. However, the ADC (p=0.023), λ_2 (p=0.023) and RD (p=0.031) of WM NBOs were significantly higher in the six patients with neurological symptoms compared to the eight patients without neurological symptoms.

Fiber Tractography

FT could be performed for adjacent WM tracts of 18/57 (32%) NBOs (Table 5). Four NBOs were located in the GM and 14 in the WM. In 15/18 cases (83%), NBOs were found to have no effect on the trajectory of the WM tracts (Figure 3). Only in three cases, did NBOs appear to disrupt the trajectory of the WM tracts (Figures 4 and 5).

Discussion

The most common CNS lesions in the brain of NF1 patients are the so-called NBOs [5,6,14]. Histopathologically these lesions represent areas of vacuolar/ spongiotic changes with increased fluid within the myelin [9]. To further investigate the microstructure and quality of the NBOs, we studied the intralesional water mobility by measuring the associated ADC values of these lesions. We found statistically significantly higher ADC values in GM NBOs and WM NBOs compared to NAS and that of matching brain regions in controls. The increase in ADC values is in concordance with the findings of Alkan et al. and Sheikh et al. (increased ADC values in NBOs compared to normal brain in controls) [12,13] and Eastwood et al. (increased ADC values in NBOs and in normal-appearing basal ganglia compared to controls) [11]. The increased ADC values may be explained by decreased cellularity or axon number and myelin sheath disorganization permitting greater extracellular water mobility/diffusivity.

Microstructural integrity can be examined more accurately by DTI. By matrix diagonalization, eigenvalues (λ_1, λ_2, λ_3) can be calculated including the corresponding anisotropy indexes [27]. Tissue anisotropy is determined by many factors including axonal packing, relative membrane permeability to water, internal axon structure, degree of myelination and overall tissue water content to mention the most important factors [27]. The degree of tissue anisotropy is quantified by FA. We found decreased FA values in GM and WM NBOs compared to NAS and that of controls. Moreover the reduction was greater for WM NBOs. Our findings are in contrast with the Results of van Engelen et al. who did not find significant

differences of FA values in NBOs compared to NAS and controls [17]. The study by Mentzel et al. also failed to find significant differences in FA values between NBOs and perilesional normal-appearing brain or that of controls [15]. They concluded that NBOs did not result in demyelination or structural disturbance or damage of fibers and axons. Our data indicate that even though NBOs may regress or disappear over time on conventional T1 and T2-weighted imaging, dysmyelination and axonal damage may be present in NBOs. This is in agreement with the Results of Tognini et al. [14]. They showed that in the region of regressed or disappeared NBOs the ADC values did not normalize. This supports the hypothesis that macroscopic disappearance of the lesions is not always associated with microscopic normalization of the tissue ultrastructure [14]. Using DTI, Ferraz-Filho et al. found lower FA values in the cerebellum of NF1 patients with NBOs compared to NF1 patients without NBOs and controls [18]. The same group showed that the decrease in FA values persists after disappearance or reduction of NBOs in the basal ganglia, cerebellum and thalami [19]. These findings are in agreement with our hypothesis that NBOs cause microstructural changes in brain regions of NF1 children and that these changes do not completely normalize after macroscopic disappearance of NBOs on conventional T1 and T2-weighted MRI.

The literature has suggested the use of eigenvalues to discriminate myelin from axonal pathologies. Axial diffusivity (AD, λ_1) measures the diffusion of water molecules parallel to the main axis of the axons. RD (the average of λ_2 and λ_3) measures the diffusion of water molecules perpendicular to the main axis of the fibers. An increased AD indicates disturbance of axons and an increased RD is believed to be related to myelin deficiency or injury [28,29]. Myelin loss and axonal damage may have a significant impact on the long-term disability of patients. Hence, a non-invasive modality which differentiates injury to myelin from axonal pathology may be very useful in evaluating and selecting therapeutic strategies for patient management [28]. RD values were significantly higher for both GM and WM NBOs compared to the NAS and controls in our study. AD showed the same trend for GM, but not for WM. Increases in AD and RD in NBOs is in agreement with the Results by van Engelen et al. [17]. Additionally, several previous studies have reported increased AD and RD in neurodegenerative conditions. These studies have suggested that both increased AD and RD may result from myelin loss in combination with axonal injury [30-32]. Our findings could be explained by myelin deficiency in both GM and WM NBOs as well as axonal disturbance in GM NBOs.

Special attention was paid to NAS in NF1 patients to determine if these regions were different from the matching brain parenchyma of healthy controls. Despite the fact that the findings were not statistically significantly different, we observed a tendency towards an increase in ADC and RD values and a decrease of FA values in GM NAS compared to controls. This suggests that the "normal-appearing" areas of NF1 are quantitatively altered for GM. However, all the WM NAS parameters (ADC, FA, AD and RD) were decreased compared to controls which appears to be a counterintuitive finding. Previous studies reported higher ADC values in normal-appearing brain regions in NF1 patients compared to controls [11,14]. Additionally, FA values in the thalami have been reported to be lower in NBOs compared to those in controls [18]. These and our Results support the hypothesis that in children with NF1 there are generalized microstructural alterations even in the absence of NBOs. The same finding was reported by Zamboni et al. in adults with NF1 [16]. These findings may explain the increased incidence of neurocognitive findings in patients with NF1.

When we compared the ADC, FA, eigenvalues and RD of the patients with and without neurological symptoms, we did not find a correlation between decreased WM NBO FA values and neurological symptoms but we did find significantly higher WM NBO values of ADC, λ_2, and RD (p value 0.023, 0.023, and 0.031 respectively) for the patients who had neurological symptoms. This result may represent the presence of white matter myelin deficiency contributing to the neurological symptoms.

FT is a powerful post-processing tool which allows the graphical reconstruction of WM tracts [23,33]. To our knowledge, the impact of involvement of the major WM tracts by NBOs has not yet been studied using FT. NBOs are expected to result in changes of the diffusion properties of WM tracts either by infiltration, tract displacement or tract disruption. The small number of patients likely prevented a demonstration of statistical significance. The majority of the NBOs had no effect on the tracts. However, three out of 18 NBOs appeared to disrupt adjacent/affected WM tracts.

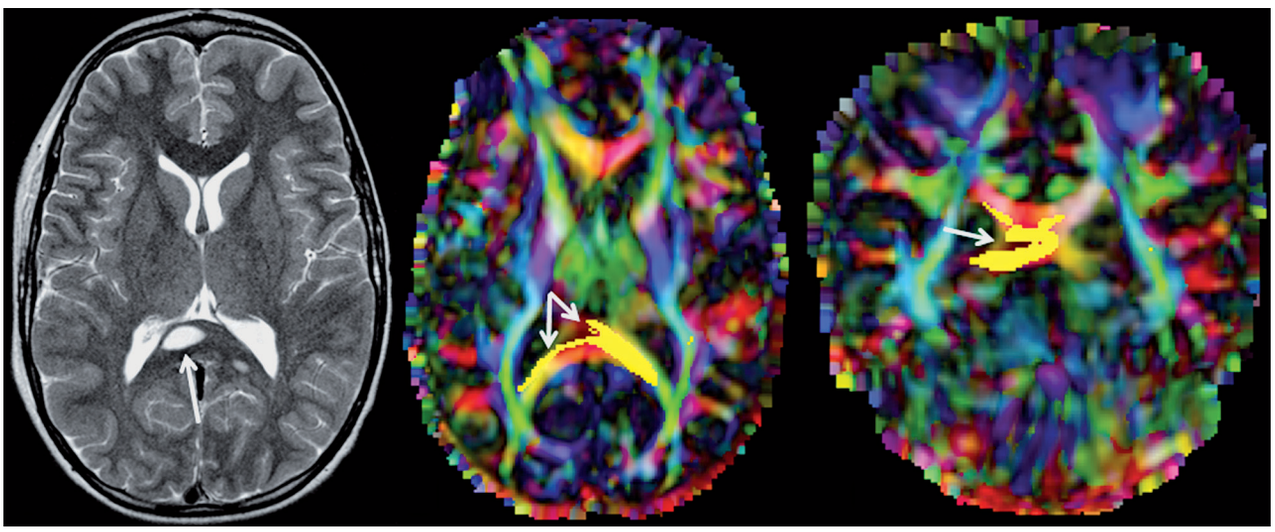

A B C

Figure 4 A) Axial T2-weighted image of patient 10 shows a NBO in the right part of the splenium of the corpus callosum (arrow). A smaller, additional NBO is seen in the right lateral part of the splenium. Axial (B) and coronal (C) color-coded FA maps with superimposed FT of the callosal fibers running through the splenium show disruption of the fibers by the NBO (arrows).

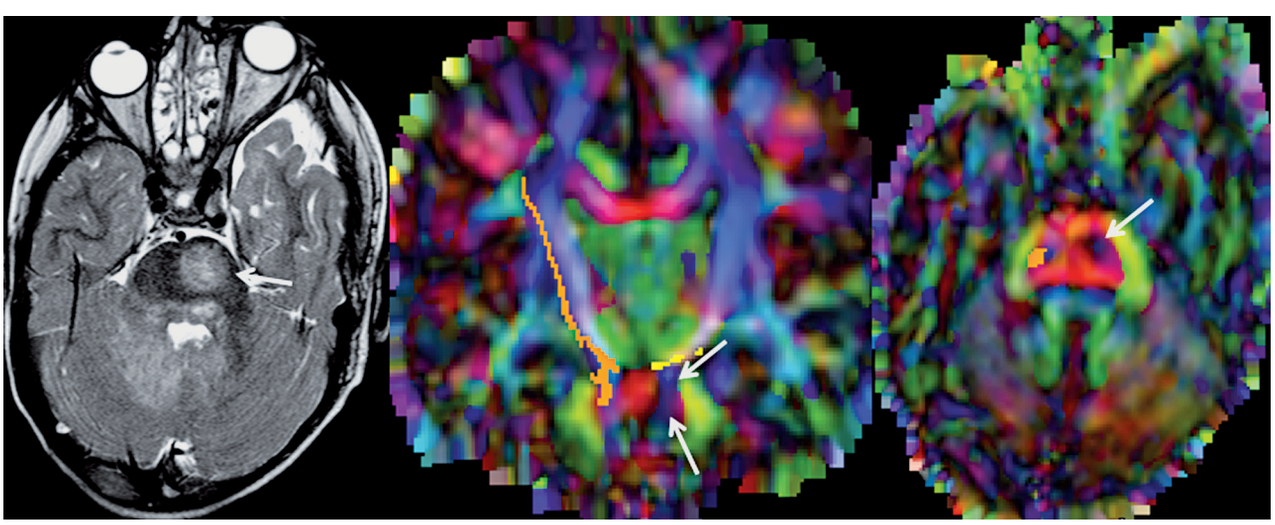

A B C

Figure 5 A) Axial T2-weighted image of patient 12 shows a NBO in the left anterior part of the pons (arrow). Additional NBOs are seen in the right middle cerebellar peduncle, bilateral dentate nuclei and left central tegmental tract. Axial (B) and coronal (C) color-coded FA maps with superimposed FT of the left (yellow) and right (orange) corticobulbar/corticospinal tracts show disruption of the fibers of the right corticobulbar/corticospinal tract by the NBO (arrows).

None of the NBOs caused a displacement of the adjacent WM tracts. The patients with disrupted tracts of deep cerebellar nuclei and splenium of the corpus callosum had neurologic symptoms, whereas the patient with disrupted corticospinal/corticobulbar tract did not show any neurologic symptoms. Some of the patients with neurologic symptoms had NBOs without any affect on the trajectories. Due to the limited number of samples, a correlation between disruption and neurological symptoms related to the affected WM tracts could not be established/evaluated in our study.

Our study suffers from several limitations. Many of the NBOs were located symmetrically in both hemispheres and were of similar size. Upon placing the ROIs to the contralateral NAS, we therefore had to adjust the location

in several cases. In addition, a selection bias of our patient population towards children is present and the study is retrospective in design. Finally, no detailed time-matched neuropsychological evaluation, follow-up examinations or pathological specimens were available. Future studies should be prospective in design to evaluate the impact of NBOs on tract development, maturation, and neurocognitive and motor function. In addition, serial follow-up examinations could also shed more light on the mystery of spontaneously vanishing NBOs.

In conclusion, increased ADC values in NBOs match the histopathological finding of myelin vacuolation and spongiotic changes attributed to increased water accumulation. Decreased FA and increased AD and RD in NBOs could be explained by a combination of myelin damage and axonal disturbance. In concordance with our hypothesis, the decrease in WM NBO FA values was greater for the GM NBOs. Increased ADC values and RD in WM NBOs could be correlated with the presence of symptoms. Unaffected tracts predominate in our study compared to three disrupted tracts out of 18. Future prospective studies, evaluating larger patient groups with special emphasis on the involvement and clinical manifestations of WM tract involvement by NBOs are mandatory to better understand the impact of NBOs on brain development and neurocognitive functions.

References

1 Williams VC, Lucas J, Babcock MA, et al. Neurofibromatosis type 1 revisited. Pediatrics. 2009; 123 (1): 124-133. doi: 10.1542/peds.2007-3204.
2 Hyman SL, Shores A, North KN. The nature and frequency of cognitive deficits in children with neurofibromatosis type 1. Neurology. 2005; 65 (7): 1037-1044. doi: 10.1212/01.wnl.0000179303.72345.ce.
3 Rogriguez FJ, Perry A, Gutmann DH, et al. Gliomas in neurofibromatosis type 1: a clinicopathologic study of 100 patients. J Neuropathol Exp Neurol. 2008; 67 (3): 240-249. doi: 10.1097/NEN.0b013e318165eb75.
4 Ghosh PS, Rothner AD, Emch TM, et al. Cerebral vasculopathy in children with neurofibromatosis type 1. J Child Neurol. 2013; 28 (1): 95-101. doi.: 10.1177/0883073812441059.
5 DeBella K, Poskitt K, Szudek J, et al. Use of "unidentified bright objects" on MRI for diagnosis of neurofibromatosis 1 in children. Neurology. 2000; 54 (8): 1646-1650. doi: 10.1212/WNL.54.8.1646.
6 Szudek J, Friedman JM. Unidentified bright objects associated with features of neurofibromatosis 1. Pediatr Neurol. 2002; 27 (2): 123-127. doi: 10.1016/S0887-8994(02)00403-4.
7 Gill DS, Hyman SL, Steinberg A, et al. Age-related findings on MRI in neurofibromatosis type 1. Pediatr Radiol. 2006; 36 (10): 1048-1056. doi: 10.1007/s00247-006-0267-2.
8 Lopes Ferraz Filho JR, Munis MP, Soares Souza A, et al. Unidentified bright objects on brain MRI in children as a diagnostic criterion for neurofibromatosis type 1. Pediatr Radiol. 2008; 38 (3): 305-310. doi: 10.1007/s00247-007-0712-x.
9 DiPaolo DP, Zimmerman RA, Rorke LB, et al. Neurofibromatosis type 1: pathologic substrate of high-signal-intensity foci in the brain. Radiology. 1995; 195 (3): 721-724.
10 Kraut MA, Gerring JP, Cooper KL, et al. Longitudinal evolution of unidentified bright objects in children with neurofibromatosis-1. Am J Med Genet A. 2004; 129A (2): 113-119. doi: 10.1002/ajmg.a.20656.
11 Eastwood JD, Fiorella DJ, MacFall JF, et al. Increased brain apparent diffusion coefficient in children with neurofibromatosis type 1. Radiology. 2001; 219 (2): 354-358. doi: 10.1148/radiology.219.2.r01ap25354.
12 Sheikh SF, Kubal WS, Anderson AW, et al. Longitudinal evaluation of apparent diffusion coefficient in children with neurofibromatosis type 1. J Comput Assist Tomogr. 2003; 27 (5): 681-686. doi: 10.1097/00004728-200309000-00004.
13 Alkan A, Sigirci A, Kutlu R, et al. Neurofibromatosis type 1: diffusion weighted imaging findings of brain. Eur J Radiol. 2005; 56 (2): 229-234. doi 10.1016/j.ejrad.2005.05.008.
14 Tognini G, Ferrozzi F, Garlaschi G, et al. Brain apparent diffusion coefficient evaluation in pediatric patients with neurofibromatosis type 1. J Comput Assist Tomogr. 2005; 29 (3): 298-304. doi: 10.1097/01.rct.0000162406.71300.b7.
15 Mentzel HJ, Karadag D, Güllmar D, et al. Unidentified bright objects in neurofibromatosis type 1: Results of diffusion tensor imaging in children and adolescents. J Pediatr Neurol. 2006; 4 (1): 27-31.
16 Zamboni SL, Loenneker T, Boltshauser E, et al. Contribution of diffusion tensor MR imaging in detecting cerebral microstructural changes in adults with neurofibromatosis type 1. Am J Neuroradiol. 2007; 28 (4): 773-776.
17 van Engelen SJ, Krab LC, Moll HA, et al. Quantitative differentiation between healthy and disordered brain matter in patients with neurofibromatosis type I using diffusion tensor imaging. Am J Neuroradiol. 2008; 29 (4): 816-822. doi: 10.3174/ajnr.A0921.
18 Ferraz-Filho JR, da Rocha AJ, Muniz MP, et al. Diffusion tensor MR imaging in neurofibromatosis type 1: expanding the knowledge of microstructural brain abnormalities. Pediatr Radiol. 2012; 42 (4): 449-454. doi: 10.1007/s00247-011-2274-1.
19 Ferraz-Filho JR, Jose da Rocha A, Muniz MP, et al. Unidentified bright objects in neurofibromatosis type 1: conventional MRI in the follow-up and correlation of microstructural lesions on diffusion tensor images. Eur J Paediatr Neurol. 2012; 16 (1): 42-47. doi: 10.1016/j.ejpn.2011.10.002.
20 Woods RP, Grafton ST, Holmes CJ, et al. Automated image registration: I. General methods and intrasubject, intramodality validation. J Comput Assist Tomogr. 1998; 22 (1): 139-152. doi: 10.1097/00004728-199801000-00027.
21 Beg MF, Miller MI, Trouvé A, et al. Computing large deformation metric mapping via geodesic flows of diffeomorphisms. Int J Comput Vision. 2005; 61 (2): 139-157. doi: 10.1023/B:VISI.0000043755.93987.aa.
22 Huang H, Ceritoglu C, Li X, et al. Correction of B0 susceptibility induced distortion in diffusion-weighted images using large-deformation diffeomorphic metric mapping. Magn Reson Imaging. 2008; 26 (9): 1294-1302. doi: 10.1016/j.mri.2008.03.005.

23 Mori S, Crain BJ, Chacko VP, et al. Three-dimensional tracking of axonal projections in the brain by magnetic resonance imaging. Ann Neurol. 1999; 45 (2): 265-269.
24 Xue R, van Zijl PC, Crain BJ, et al. In vivo three-dimensional reconstruction of rat brain axonal projections by diffusion tensor imaging. Magn Reson Med. 1999; 42 (6): 1123-1127.
25 Huang H, Zhang J, van Zijl PC, et al. Analysis of noise effects on DTI-based tractography using the brute-force and multi-ROI approach. Magn Reson Med. 2004; 52 (3): 559-565. doi: 10.1002/mrm.20147.
26 Wakana S, Caprihan A, Panzenboeck MM, et al. Reproducibility of quantitative tractography methods applied to cerebral white matter. Neuroimage. 2007; 36 (3): 630-644. doi: 10.1016/j.neuroimage.2007.02.049.
27 Basser PJ, Jones DK. Diffusion-tensor MRI: theory, experimental design and data analysis - a technical review. NMR Biomed. 2002; 15 (7-8): 456-467. doi: 10.1002/nbm.783.
28 Song SK, Sun SW, Ramsbottom MJ, et al. Dysmyelination revealed through MRI as increased radial (but unchanged axial) diffusion of water. Neuroimage. 2002; 17 (3): 1429-1436. doi: 10.1006/nimg.2002.1267.
29 Nair G, Tanahashi Y, Low HP, et al. Myelination and long diffusion times alter diffusion-tensor-imaging contrast in myelin-deficient shiverer mice. Neuroimage. 2005; 28 (1): 165-174. doi: 10.1016/j.neuroimage.2005.05.049.
30 Pierpaoli C, Barnett A, Pajevic S, et al. Water diffusion changes in Wallerian degeneration and their dependence on white matter architecture. Neuroimage. 2001; 13 (6 Pt 1): 1174-1185. doi: 10.1006/nimg.2001.0765.
31 Lowe MJ, Horenstein C, Hirsch JG, et al. Functional pathway-defined MRI diffusion measures reveal increased transverse diffusivity of water in multiple sclerosis. Neuroimage. 2006; 32 (3): 1127-1133. doi: 10.1016/j.neuroimage.2006.04.208.
32 Trip SA, Wheeler-Kingshott C, Jones SJ, et al. Optic nerve diffusion tensor imaging in optic neuritis. Neuroimage. 2006; 30 (2): 498-505. doi: 10.1016/j.neuroimage.2005.09.024.
33 Ciccarelli O, Catani M, Johansen-Berg H, et al. Diffusion-based tractography in neurological disorders: concepts, applications, and future developments. Lancet Neurol. 2008; 7 (8): 715-727. doi: 10.1016/S1474-4422(08)70163-7.

Thierry A.G.M. Huisman, MD
Professor of Radiology, Pediatrics and Neurology
Director of Pediatric Radiology and Pediatric Neuroradiology
Division of Pediatric Radiology, The Russell H. Morgan
Department of Radiology and Radiological Science
The Johns Hopkins School of Medicine
Charlotte R. Bloomberg Children's Center
Sheikh Zayed Tower, Room 4174
1800 Orleans Street
Baltimore, MD 21287-0842, USA
Tel.: +14109556454
Fax: +14105023633
E-mail: thuisma1@jhmi.edu